



Effect of Substrate Microstructure on Thermocapillary Flow and Heat Transfer of Nanofluid Droplet on Heated Wall

Yanni Jiang¹ · Faxuan Chi¹ · Qisheng Chen² · Xiaoming Zhou¹

Received: 23 January 2021 / Accepted: 4 May 2021 / Published online: 18 May 2021
© The Author(s), under exclusive licence to Springer Nature B.V. 2021

Abstract

In order to reveal the effect of substrate microstructure on heat transfer of nanofluid droplet evaporation, the thermocapillary flow characteristics and heat transfer performance of nanofluid droplet on different substrates are investigated. The two-phase mixture model is used to simulate the nanofluid flow, and three kinds of micro-structured substrates (namely, sawtooth, rectangle, and parabola structures) are considered. The computational results show that micro-structured substrate can affect the temperature and flow field distributions inside the droplet, and the petal structure of isotherm and flow velocity of smooth substrate is larger than that with micro-structured substrates. The average heat flux at droplet surface increases with substrate temperature increasing, the average heat flux with rectangle substrate is larger than smooth substrate, while that of sawtooth and parabola substrate is smaller. With the increase of nanoparticle volume fraction the average heat flux at droplet surface almost increases linearly.

Keywords Droplet · Substrate microstructure · Nanofluid · Thermocapillary convection · Two-phase mixture model · Heat transfer

Nomenclature

a	Acceleration, m^2/s
C_p	Specific heat, J/kgK
C_B	Boltzmann's constant, $1.38066 \times 10^{-23} J/K$
D	Diameter of droplet, m
d_p	Nanoparticle diameter, nm
f	Friction factor
f_{drag}	Drag function
g	Gravitational acceleration, m/s^2
h	Height of microstructure, m
L	Width of microstructure, m
Ma	Marangoni number
n	Normal direction
Nu	Nusselt number
P	Pressure, Pa
Pr	Prandtl number
Pr	$C_p \mu / \lambda$
Re_p	Nanoparticle Reynolds number

S_{gen}	Entropy generation (W/m^3K)
T	Fluid temperature, K
T_a	Ambient temperature, K
T_w	Bottom temperature, K
\vec{v}	Velocity vector (m/s)
u	X-axis velocity component (m/s)
v	Y-axis velocity component (m/s)
x	X-axis coordinate (m)
y	Y-axis coordinate (m)
λ	Thermal conductivity, W/mK
γ_T	Surface tension temperature coefficient, N/mK
α_p	Nanoparticle volume fraction
μ	Dynamic viscosity, kg/ms
ρ	Density, kg/m^3
π	Circumference ratio
ΔT	System temperature difference
\emptyset	Variables
ave	Average value
f	Base fluid
fr	Freezing
nf	Nanofluid
p	Nanoparticles
w	Substrate wall
a	Ambient temperature

✉ Xiaoming Zhou
xmzhou@hhu.edu.cn

¹ College of Mechanical and Electrical Engineering, Hohai University, Changzhou, China

² Institute of Mechanics, Chinese Academy of Sciences, Beijing, China

Introduction

The droplet evaporation plays a significant role in a lot of practical applications, e.g. spray cooling (Bhattacharya et al. 2009), inject printing (Ren et al. 2012), surface coating (Paria et al. 2014), and so on. In the process of droplet evaporation, the liquid evaporation at the edge is faster than that at the top. The nonuniform evaporation rate of droplet leads to the nonuniform surface temperature distribution, which leads to the uneven surface tension, then thermocapillary convection will be induced in the interior of droplet. Due to the small size of the droplet and the weak buoyancy convection effect, the thermocapillary convection plays a dominant role in the droplet evaporation, so numerous investigations focus on the thermocapillary flow in droplet have been conducted. Deegan et al. (1997) found that Marangoni convection effect leads to the formation of coffee ring deposition after the droplet containing solid particles evaporated on the plane. Hu and Larson (2005) found that when the contact angle is greater than 14° the convection flows from the edge to the top, while when the contact angle is less than 14° the flow direction flows from the top to the edge. Xu (2007) found that there is a stagnation point on the surface of the droplet, and the flow direction of the droplet is opposite on both sides of the stagnation point. Moreover, in the droplet containing with different volatile liquids, various thermal patterns induced by thermal flow have been found, including hydrothermal waves and cellular structure waves et al. (Sefiane et al. 2008; Ye et al. 2018). Sefiane et al. (2013) confirmed that hydrothermal waves in evaporating droplets are bulk waves. Recently, Ye et al. (2020) experimentally studied the evolution of thermal patterns and the variation of evaporation rate during water and ethanol droplet evaporation at low pressures. Gao et al. (2020) experimentally investigated the dynamic characteristics of droplet evaporation at a constant heat flux condition.

In addition to the effect of thermocapillary convection on droplet evaporation, the properties of the substrate are also an important factor, and this research has attracted the interest of many researchers. Saada et al. (2013) numerically studied the influence of substrate thermophysical properties on droplet evaporation surface temperature distribution and liquid phase concentration distribution, and found that the thinner the substrate, the greater the thermal conductivity, the faster the evaporation. Pham and Kumar (2019, 2017) investigated the drying of droplet on a rough substrate, the results show that the pinning of droplets attributed to the competition between the capillary-pressure and disjoining-pressure gradients. Zhang et al. (2014) found that coffee-ring phenomenon of droplet on rough substrate is more obvious than that on smooth substrate,

and the cross-section of the ring is wedge-shaped with its thickest part on the edge. Lohani and Sarkar (2018) studied the effect of nanoscale roughness on pattern formation, and they found that with the increase of nanoscale roughness the wetting property decreases. Darbha et al. (2012) studied the deposition of latex colloids on a nanopatterned surface, and they found that the impact of surface roughness on retention is more significant for smaller colloid. Recently, Wang et al. (2020) investigated the evaporation process and deposition pattern of saline droplet on a copper substrate with different roughness, they found that evaporation pattern of droplets has a strong relationship to substrate roughness. Dou and Hao (2021) numerically studied the evaporation processes of sessile droplets on both heated flat and structured hydrophobic surfaces, and the contact-line dynamics and heat transfer regarding the evaporation of droplets are simulated and the effects of the heat conductivity, wettability, and roughness of the substrate on the droplet evaporation are investigated. Moreover, some investigators also focus on the wetting of droplet on different micro-structured substrate, e.g. Gong et al. (2017), Zu et al. (2010) and Yu et al. (2016, 2019, 2020).

Above all, the flow pattern in the droplet and the effect of rough substrate on the wetting of droplet have received much attentions, however, the investigation of the flow and heat transfer of droplet on micro-structured substrate is still lacking, in particular about the effect of different microstructures at substrate surface. Subsequently, the objective of the article is to reveal the effect of micro-structured substrate on thermocapillary flow and heat transfer performance of nanofluid droplet, and the effect of nanoparticle concentration on heat transfer is also discussed.

Physical and Mathematical Model

The research model is shown in Fig. 1, in which a semicircular droplet is located on heated substrate, and the diameter of droplet $D = 5$ mm. The temperature of substrate is T_w , the ambient temperature around droplet is T_a . The wetting mode of droplet on substrate surface is Wenzel mode, and the contact angle is $\pi/2$. Three kinds of micro-structured surface with sawtooth, rectangle and parabola structures are considered in this paper, and the smooth surface is used as reference substrate. The microstructure shapes are shown in Fig. 2, where $l = 0.02$ mm and $h = 0.01$ mm. The working fluid of droplet is nanofluid silicone oil- Al_2O_3 . In order to investigate the substrate structure on flow and heat transfer of droplet, we assume the volume and shape of droplet remains a steady state, and the heat exchange with surrounding environment at droplet surface is natural convection heat transfer. Moreover, in order to simplify the computational

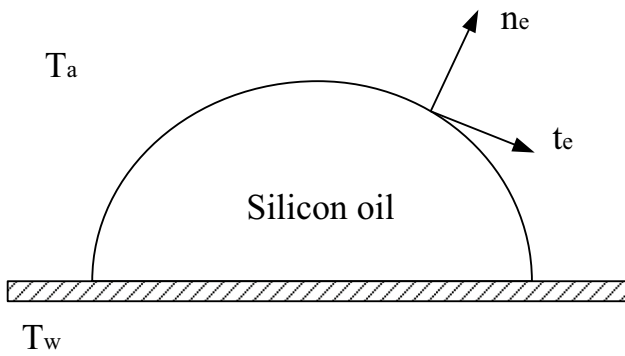


Fig. 1 Physical model

model, we assume that: 1) the surface tension of nanofluids is a linear function of temperature; 2) the thermophysical properties of basic fluid remain constant; 3) the flow in the droplet is a laminar flow. In the simulation, two-phase mixing model is used to describe the nanofluid flow, then the governing equations of nanofluid thermocapillary flow and heat transfer in droplet are described as follows.

Continuity equation:

$$\nabla \cdot (\rho_{nf} \vec{V}_{nf}) = 0 \tag{1}$$

Momentum equation:

$$\begin{aligned} \nabla \cdot (\rho_{nf} \vec{V}_{nf} \vec{V}_{nf}) = & -\nabla P_{nf} + \nabla \cdot (\mu_{nf} \nabla \vec{V}_{nf}) \\ & + \nabla \cdot (\alpha_p \rho_p \vec{V}_{dr,p} \vec{V}_{dr,p}) \\ & + \nabla \cdot ((1 - \alpha_p) \rho_f \vec{V}_{dr,f} \vec{V}_{dr,f}) \end{aligned} \tag{2}$$

Energy equation:

$$\nabla \cdot [(\alpha_p \rho_p c_{p,p} \vec{V}_p + (1 - \alpha_p) \rho_f c_{p,f} \vec{V}_f) T] = \nabla \cdot (\lambda_{nf} \nabla T) \tag{3}$$

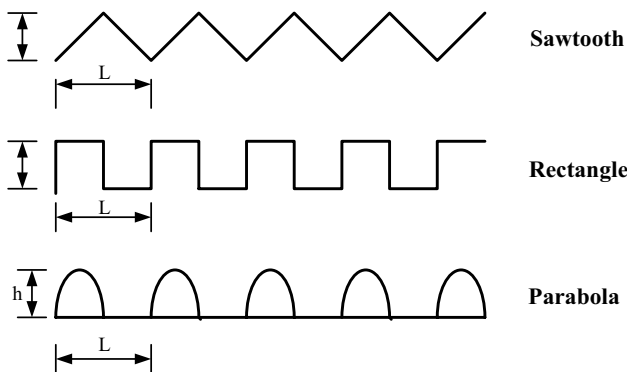


Fig. 2 The shapes of droplet substrate structure

Volume fraction equation:

$$\nabla \cdot (\alpha_p \rho_p \vec{V}_{nf}) = -\nabla \cdot (\alpha_p \rho_p \vec{V}_{dr,p}) \tag{4}$$

Where $\vec{V}_{nf} = \frac{\alpha_p \rho_p \vec{V}_p + (1 - \alpha_p) \rho_f \vec{V}_f}{\rho_{nf}}$ and $\vec{V}_{dr,p} = \vec{V}_p - \vec{V}_{nf}$ are the mass-averaged velocity and drift velocity respectively, and α_p denotes nanoparticle concentration.

The slip velocity is the velocity of nanoparticle (the second phase) relative to that of basic fluid (the primary phase):

$$\vec{V}_{pf} = \vec{V}_p - \vec{V}_f \tag{5}$$

The relation of the drift velocity and the slip velocity is written as:

$$\vec{V}_{dr,p} = \vec{V}_{pf} - \frac{\alpha_p \rho_p}{\rho_{nf}} (\vec{V}_f - \vec{V}_p) \tag{6}$$

The slip velocity is obtained according to Eq. (6) (1996), and the drag function f_{drag} is computed by Eq. (7) (Schiller and Naumann 1935).

$$\vec{V}_{pf} = \frac{\rho_p d_p^2}{18 \mu_f f_{drag}} \frac{\rho_p - \rho_f}{\rho_p} \vec{a} \tag{7}$$

$$f_{drag} = \begin{cases} 1 + 0.15 Re_p^{0.687} & Re_p \leq 1000 \\ 0.0183 Re_p & Re_p > 1000 \end{cases} \tag{8}$$

where $Re_p = V_{nf} d_p \rho_{nf} / \mu_{nf}$ and \vec{a} in Eq. (6) are written as $\vec{a} = \vec{g} - (\vec{V}_{nf} \nabla) \vec{V}_{nf}$.

Nanofluid Thermophysical Properties

Accurate description of nanofluid thermophysical properties is very important for numerical simulation. The investigation of Das et al. (2008) showed that the rule of mixture is not suitable for nanofluid, thus the calculation of nanofluid thermal physical parameters need more precise models. In our article, the computation of nanofluid density and specific heat are expressed as:

$$\rho_{nf} = \alpha_p \rho_p + (1 - \alpha_p) \rho_f \tag{9}$$

$$(\rho c_p)_{nf} = \alpha_p (\rho c_p)_p + (1 - \alpha_p) (\rho c_p)_f \tag{10}$$

Based on the rule proposed by Das et al. (2008), the Eq. (8) is used as density computation of nanofluid. Utilizing the hypothesis of heat balance between the base fluid and nanoparticles (Khanafer and Vafai 2011), Eq. (9) is used for the calculation of specific heat.

Table 1 Thermal physical parameters of base fluid and nanoparticle

Thermal physical parameters Basic fluid and particles	$\rho(\text{kg/m}^3)$	$c_p(\text{J/kgK})$	$\lambda(\text{W/m K})$	$\mu(\text{m}^2/\text{s})$	$\gamma_T(\text{N/mK})$
Basic fluid (silicon oil)	950	1630	0.14	0.019	-6.23×10^{-5}
Nanoparticles (Al_2O_3)	3950	773	36	/	/

The computation of nanofluid dynamic viscosity and thermal conductivity is based on Eqs. (11) and (12) respectively, which is derived by Corcione (2012, 2011) and based on a lot of experimental data. The effect of nanoparticles concentration and size is included in the models, and the models are expressed as follows:

$$\lambda_{nf} = \lambda_f \left[1 + 4.4 \cdot \text{Re}_p^{0.4} \cdot \text{Pr}^{0.66} \cdot \left(\frac{T}{T_{fr}}\right)^{10} \cdot \left(\frac{\lambda_p}{\lambda_f}\right)^{0.03} \cdot \alpha_p^{0.66} \right] \tag{11}$$

$$\mu_{nf} = \frac{\mu_f}{1 - 24.3745 \cdot d^{-0.264} \cdot \alpha_p^{1.028}} \tag{12}$$

Where, Pr is Prandtl number of basic fluid, Re_p is nanoparticles Reynolds number (Das et al. 2008):

$$\text{Re}_p = \frac{2 \cdot \rho_f \cdot C_B \cdot T}{\pi \cdot \mu_f^2 \cdot d} \tag{13}$$

Entropy Production

Entropy production refers to the irreversibility of the actual thermodynamic process. There are two kinds of effects related to convective heat transfer, namely, heat transfer and flow friction. The computational equation of local entropy production is written as:

$$S_{gen} = \frac{\lambda_{nf}}{T^2} \left[\left(\frac{\partial T}{\partial x}\right)^2 + \left(\frac{\partial T}{\partial y}\right)^2 \right] + \frac{\mu_{nf}}{T} \left[2 \cdot \left\{ \left(\frac{\partial u}{\partial x}\right)^2 + \left(\frac{\partial v}{\partial y}\right)^2 \right\} + \left(\frac{\partial u}{\partial y} + \frac{\partial v}{\partial x}\right)^2 + \left(\frac{\partial u}{\partial x} + \frac{\partial v}{\partial y}\right)^2 \right] \tag{14}$$

Where, u , and v denote nanofluid velocity component at x axis and y axis, respectively.

Boundary Condition

$$u = v = 0, T = T_{w \text{ at substrate surface}} \tag{15}$$

$$u \times n = 0, \mu \frac{\partial u}{\partial n} = \gamma_T \nabla T, q = h \cdot (T_a - T) \text{ at droplet surface} \tag{16}$$

Table 2 The check of mesh independence (silicon oil- Al_2O_3 , $\alpha_p = 5\%$, $\Delta T = 10$ K)

grid numbers	12,700	21,120	42,467	101,952
Physical properties				
Maximal velocity (m/s)	4.123×10^{-7}	4.321×10^{-7}	4.345×10^{-7}	4.349×10^{-7}

Where $h = \frac{k}{D} \left(2 + \frac{0.589 \text{Ra}_D^{1/4}}{\left(1 + \left(\frac{0.469}{\text{Pr}}\right)^{9/16}\right)^{4/5}} \right)$ (Incropera et al. 2006),

$$\text{Ra}_D = \frac{g \alpha_p \rho^2 C_p |T - T_a| D^3}{k \mu}$$

The non-dimensional numbers used in the present paper are expressed as follows:

Nusselt number Eq. (17),

$$\text{Nu} = -\frac{\lambda_{nf}}{\lambda_f} \cdot \left(\frac{\partial T}{\partial n} \cdot \frac{D}{T_w - T_a} \right) \tag{17}$$

Average Nusselt number Eq. (18),

$$\text{Nu}_{ave} = \frac{1}{l} \cdot \int \text{Nu}(x) dl \tag{18}$$

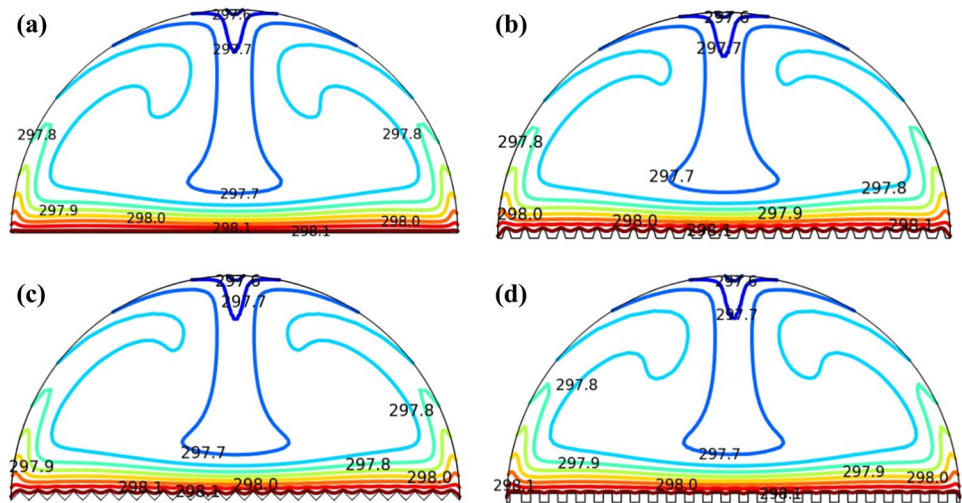
Nanofluid Thermophysical Parameters

The nanofluid used in the numerical simulations is silicon oil- Al_2O_3 , which consists of silicon oil and Al_2O_3 nanoparticles, and the nanoparticles concentration increase from 0 to 0.05. The related parameters of silicon oil and Al_2O_3 nanoparticles are shown in Table 1.

Solution Method

The equations of nanofluid flow in the droplet are discretized by the finite volume method, the diffusion terms are discretized using 2nd order central-difference schemes, and the discretization of convective term by QUICK scheme. The solving of pressure-velocity coupling is by the PISO algorithm. A non-uniform grid distribution is applied to the discretization of the computational region, and the mesh is refined at the region near droplet surface

Fig. 3 Temperature distribution in droplet as $\Delta T = 5$ K and $\alpha_p = 0.02$ ((a) smooth, (b) parabola, (c) sawtooth, (d) rectangle)



and bottom wall. In order to check the mesh independence, four types of mesh with 12,700 · 21,120 · 42,467 and 101,952 cells are tested, and the computational results of maximal velocity in the flow field are given in Table 2. We can see that the mesh 42,467 is sufficient for the solving of nanofluid flow in the droplet. The convergence criterion of computational process is 10^{-5} , namely the relative error of the variables is satisfied with the equation $|\varnothing^{n+1} - \varnothing^n|_{max} \leq 10^{-5}$, in which n denotes the iteration number and \varnothing represents the variables to be solved. The validity of the numerical method can refer to our previous papers (Jiang and Zhou 2020, 2019a, 2019b; Jiang and Xu 2017; Zhou et al. 2019).

Results and Discussions

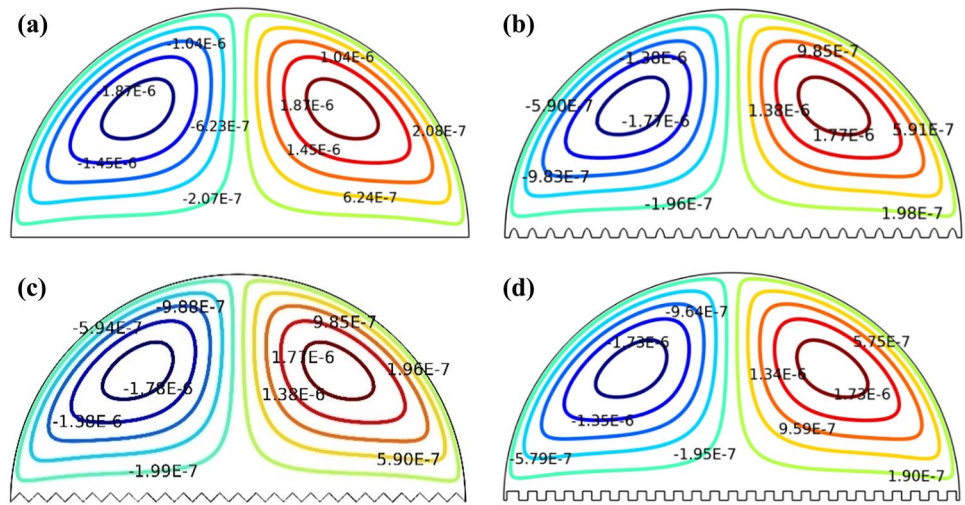
Figure 3 shows the internal temperature contours distribution in droplet on different microstructured substrates as $\Delta T = 5$ K and $\alpha_p = 0.02$. It can be seen that the temperature distribution for the four cases show the same pattern, and exists a obvious gradient distribution at the vicinity of substrate, which indicates that at the region near substrate the heat conduction is dominant. In the upper region the isotherm contours manifest as a petal structure, this is due to the stonger thermocapillary effect at droplet surface, the hot fluid is transported from the bottom to the top region. Comparing the temperature distribution of droplet on different microstructured substrates, it can be seen that the effect of microstructure is maily reflected in the upper region of the droplet, e.g. the petal structure pattern of isotherm line as $T = 297.8$ K. The petal structure of the droplet on smooth subatrate is the largest, that of rectangular substrate is the second, and that of parabola and sawtooth substrates is relatively smaller. This means that the convective heat transfer effect of droplet on smooth substrate

is the strongest, that of parabola and sawtooth substrates is weaker. Moreover, the petal structure of parabola and sawtooth substate is almost the same.

Figure 4 gives the stream function distribution inside the droplet as $\Delta T = 5$ K and $\alpha_p = 0.02$, in which the unit of stream fuction is 1/s. We can see that there are two convective vortices in the interior of droplet, in which the left vortex is clockwise circulation and the right one is counter clockwise circulation, and this flow pattern is caused by the thermocapillary effect at surface. Due to surface tension decreases with the increase of temperature, the surface tension of the droplet at the vicinity of substrate is smaller, and this leads to the surface flow is from the bottom to the top, and finally two counter rotating convective vortices are formed in droplet. Furthermore, the stream function of droplet on smooth substrate is the largest, this means that the application of micro-structured substrate can leads to the decrease of thermocapillary convection intensity. This is due to the heat transfer between nanofluid and substrate is enhanced by microstructure, and cause the decrease of temperature gradient at droplet free surface, then the thermocapillary effect at droplet surface is reduced. For different micro-structured substrates, the convection intensity of the three structures has similar value, in which the maximal stream function value of rectangle structure substrate is the smallest.

Figure 5 shows the local entropy generation distribution in droplet as $\Delta T = 5$ K and $\alpha_p = 0.02$, in which the unit of local entropy generation is W/m^3K . In general, the local entropy generation near the substrate is larger, which is mainly due to the heat exchange between fluid and substrate, and the temperature gradient in this region is larger. As different micro-structured substrates are used, the maximum value of local entropy generation increases and its distribution pattern is changed. For the smooth substrate, the larger value of local entropy generation is located at the center region

Fig. 4 Stream function distribution inside the droplet as $\Delta T = 5$ K and $\alpha_p = 0.02$ ((a) smooth, (b) parabola, (c) sawtooth, (d) rectangle)



of substrate. However, for micro-structured substrate, that is mainly distributed at the vicinity of the microstructure. This is mainly due to the heat transfer is enhanced by the substrate microstructure. Moreover, the maximum value of entropy generation of parabola substrate is the largest, and followed by triangular, rectangular and smooth substrates respectively, in which the local entropy generation of rectangular substrate is slightly larger than that of smooth substrate.

Figures 6 and 7 show the distribution of temperature and velocity at droplet surface as $\Delta T = 5$ K and $\alpha_p = 0.02$, respectively. It can be seen that there is a lowest temperature and velocity stagnation point at the middle region of droplet free surface, which is caused by the convection structure

inside the droplet due to thermocapillary effect. In Fig. 4, the convective vortex at the left side is clockwise and that at the right side is counter clockwise, this flow pattern leads to the center region of free surface is the intersection point of the left and right free surface flow, so the flow velocity is lowest. Under the action of thermocapillary effect, the heat from the substrate is transported along the free surface to the highest point of the droplet. During the transportation process, the hot fluid exchanges with the cold fluid inside the droplet, so the temperature gradually decreases along free surface, and the temperature decreases to the lowest value when it reaches the highest point of the free surface. As for the effect of substrate microstructure, the free surface

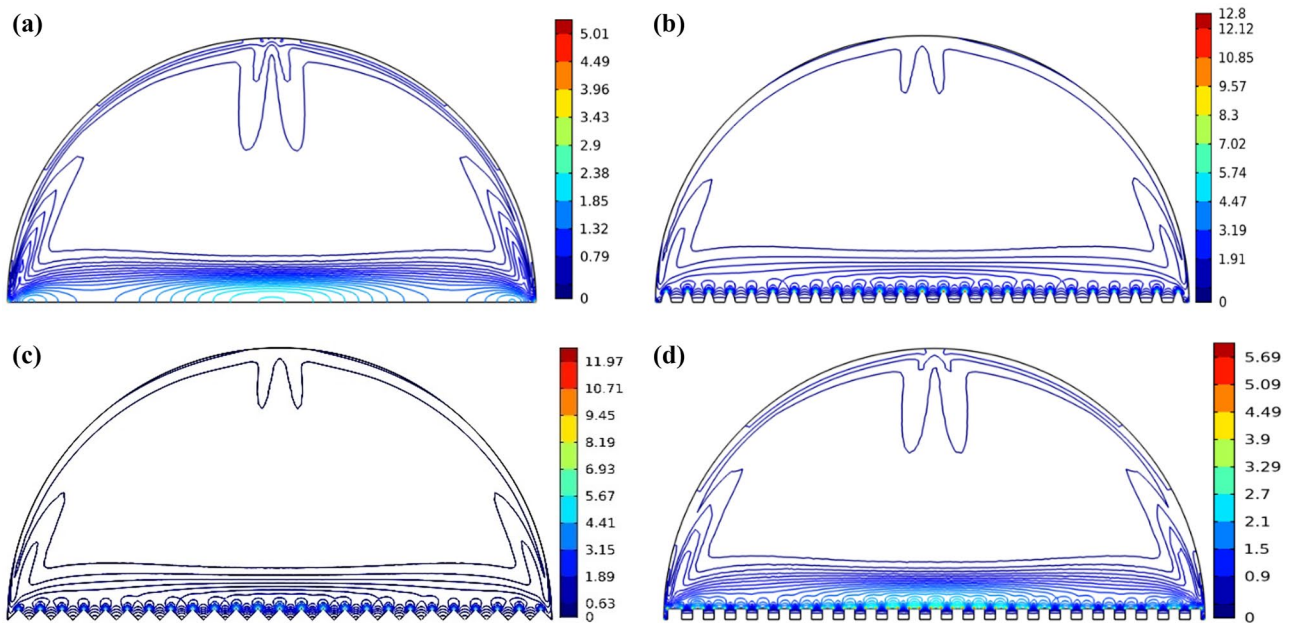


Fig. 5 Local entropy generation distribution inside the droplet as $\Delta T = 5$ K and $\alpha_p = 0.02$ ((a) smooth, (b) parabola, (c) sawtooth, (d) rectangle)

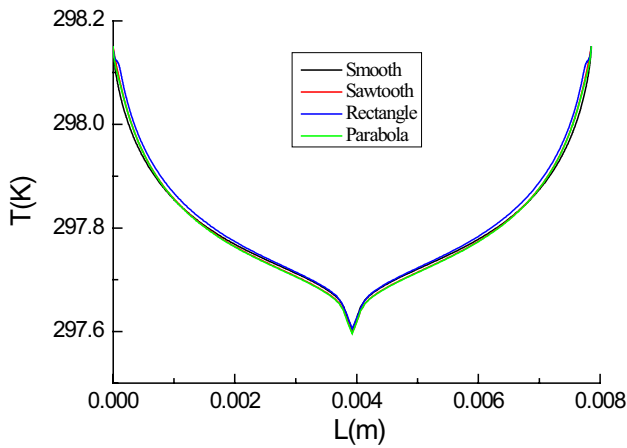


Fig. 6 Temperature distribution at droplet free surface as $\Delta T = 5$ K and $\alpha_p = 0.02$

temperature of rectangle substrate is the highest, and that of parabola substrate is the lowest. The effect of substrate microstructure on free surface velocity is more significant, as shown in Fig. 7. The free surface velocity with smooth substrate is greater than that of micro-structured substrate, and that of rectangular substrate is the smallest. The reason is that the rectangular substrate has the strongest effect on heat transfer, and resulting in a smaller temperature gradient at the free surface and a weaker thermocapillary effect. Moreover, the local velocity distribution near contact point is shown in Fig. 7(b), due to the influence of the microstructure, the local velocity changes sharply in the case with rectangular structure.

Figure 8 shows the local Nusselt number distribution at substrate surface with different micro-structured substrates as $\Delta T = 5$ K and $\alpha_p = 0.02$. For the smooth substrate, the local Nusselt number of the bottom surface is a smooth wavy curve, and its value at the periphery is obvious larger than the other region. The reason is that under the action of thermocapillary effect at free surface, there is a larger

temperature gradient the periphery region, which leads to the local Nusselt number is larger. With micro-structured substrates, the local Nusselt number becomes more uniform distribution characteristics than that of smooth substrate, and the distribution line indicates a periodic change along the substrate. In particular, the heat exchange at the central region of substrate is enhanced by microstructure, but the local valley is less than the Nusselt number of the corresponding position of smooth substrate. This variation trend shows that the heat transfer between the droplet and the substrate can be enhanced locally by using microstructures, but whether the heat transfer of the whole droplet can be enhanced depends on the average Nusselt number of the whole microstructure surface. Comparing the three kinds microstructure, the peak value of local Nusselt number of parabola structure is greater than that of sawtooth and rectangle structures.

In order to further analyze the effect of substrate microstructure on droplet heat transfer, Fig. 9 shows the relationship between the average Nusselt number of substrate surface and temperature difference for different micro-structured substrate. In general, the average Nusselt number at the substrate surface almost increases linearly with the increase of temperature difference. The average Nusselt number with smooth substrate is larger than that of micro-structured substrates, in which the sawtooth structure is the second, parabola structure is the third, and rectangle structure is the smallest. This is because the microstructures can enhance the heat exchange between the droplet and the substrate, so that the fluid temperature at the bottom of droplet is higher than that with smooth substrate and the temperature gradient is reduced.

Figure 10 shows heat flux distribution at droplet free surface with different micro-structured substrates as $\Delta T = 5$ K and $\alpha_p = 0.02$. The whole distribution pattern of heat flux is similar to that of temperature distribution, this is due to the natural convective heat transfer at droplet surface is related

Fig. 7 Velocity distribution at droplet surface as $\Delta T = 5$ K and $\alpha_p = 0.02$ ((a) velocity distribution at whole free surface, (b) local velocity distribution near contact line)

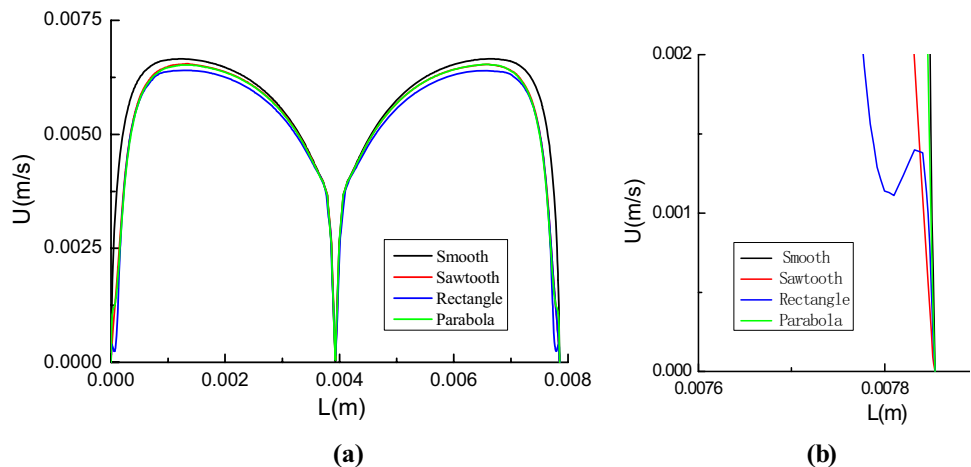
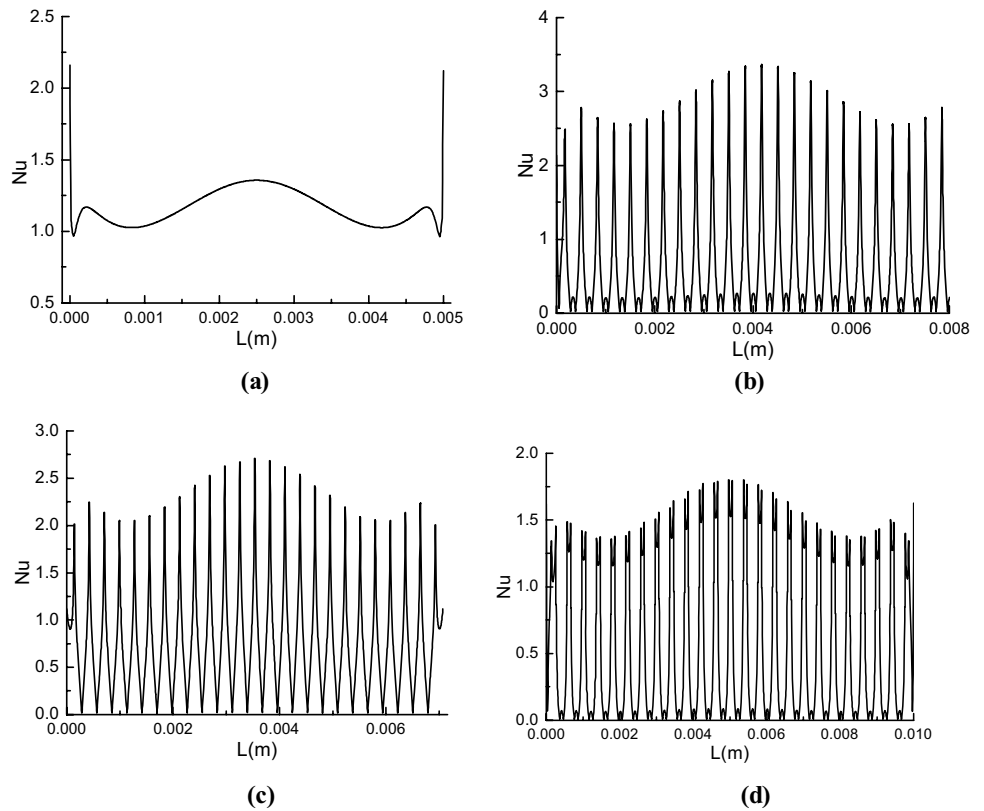


Fig. 8 Local Nusselt number distribution at substrate surface as $\Delta T=5$ K and $\alpha_p=0.02$ ((a) smooth, (b) parabola, (c) sawtooth, (d) rectangle)



to the surface temperature. For the droplet with different substrates, the heat flux of rectangle structure substrate is higher than other substrates at the whole droplet surface. However, the heat flux of sawtooth and parabola structure substrates is larger than that of smooth substrate at the peripheral region, at the central region the former is less than the later.

Figure 11 shows the variation of average heat flux at free surface with temperature difference for different substrates.

In general, with the increase of temperature difference, the free surface heat flux increases linearly. From the local enlarged figure, the heat flux at droplet free surface with rectangle structure substrate is significantly greater than other substrates, this indicates the rectangle structure is the most favorable for droplet heat transfer, and this microstructure effectively enhances the heat exchange between the fluid and substrate. Therefore, the rectangle structure substrate can be regarded as the best surface structure to enhance the droplet

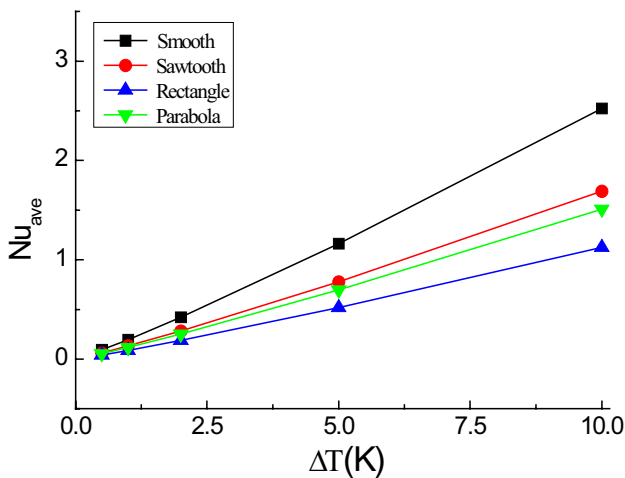


Fig. 9 Variation of average Nusselt number at substrate surface as $\Delta T=5$ K and $\alpha_p=0.02$

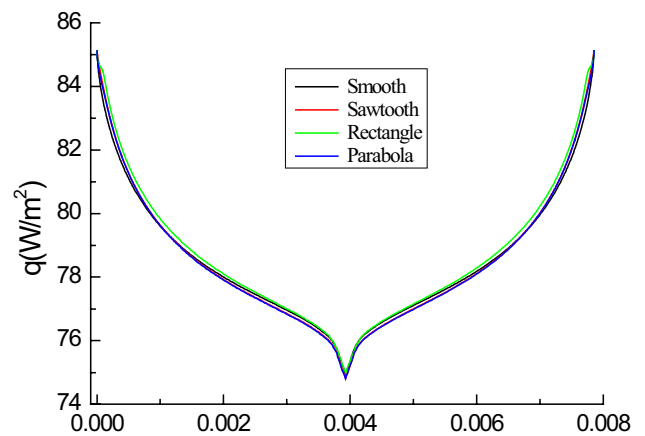


Fig. 10 Heat flux at droplet surface with different micro-structured substrates as $\Delta T=5$ K and $\alpha_p=0.02$

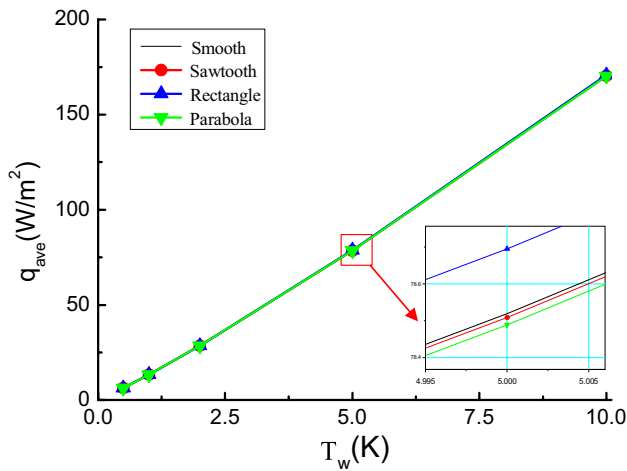


Fig. 11 Variation of average heat flux at droplet surface with temperature difference as $\alpha_p=0.02$

evaporation heat transfer. In addition, the free surface heat flux of sawtooth and parabola structure substrates is less than that of smooth substrate, this means the micro-structured substrate is not always enhance the droplet heat transfer.

Figure 12 shows the variation of average heat flux at free surface with nanoparticles volume fraction for different substrates. It can be seen that, the average heat flux at droplet free surface of rectangle structure substrate is larger than that of smooth substrate, while that of sawtooth and parabola structure substrate is less than that of smooth substrate. With the increase of nanoparticles volume fraction, the average heat flux almost increases linearly, this indicates that the droplet heat transfer can be improved by increasing concentration of nanoparticles volume fraction appropriately.

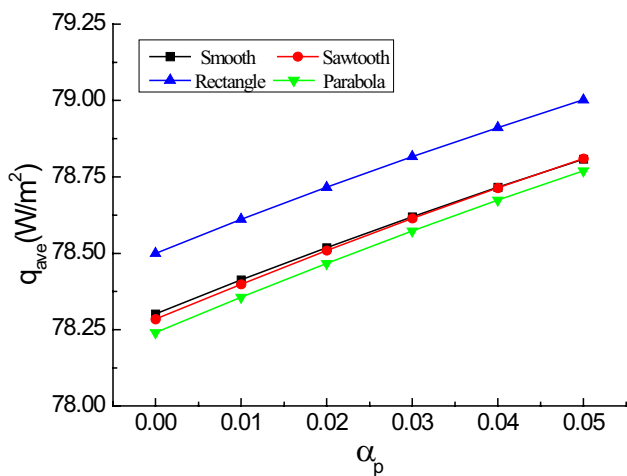


Fig. 12 Variation of average heat flux at droplet surface with nanoparticles volume fraction as $\Delta T=5\text{ K}$

Conclusions

Effect of substrate microstructure on thermocapillary convection and heat transfer of droplet was investigated in this paper, and the influence of substrate temperature and nanoparticle concentration on heat transfer are analyzed. The conclusions are obtained as follows:

- 1) Micro-structured substrate can affect the temperature and flow field distribution in droplet, and the petal structure and flow velocity of droplet on smooth substrate is the larger than that of micro-structured substrates.
- 2) The average heat flux at droplet surface increases with substrate temperature increasing, and the average heat flux with rectangle substrate is larger than smooth substrate, while that of sawtooth and parabola substrate is smaller. The rectangle structure substrate is most beneficial to the enhancement of droplet heat transfer.
- 3) The average Nusselt number at the bottom of droplet of smooth substrate is larger than that of micro-structured substrates, in which the sawtooth structure is the second, parabola structure is the third, and rectangular structure is the smallest.
- 4) With the increase of nanoparticles volume fraction the average heat flux almost increases linearly, and the droplet heat transfer can be improved by increasing concentration of nanoparticles volume fraction appropriately.
- 5) For the smooth substrate, the larger value of local entropy generation is located at the center region of substrate, while for micro-structured substrate the larger value of local entropy generation is mainly distributed in the vicinity of the microstructure.

Acknowledgments The work was supported by National Natural Science Foundation of China (No.51976080), the Fundamental Research Funds for the Central Universities (No. B200201036), and the Changzhou science and technology plan (Applied Basic Research) projects (CJ20200069).

References

Bhattacharya, P., Samanta, A., Chakraborty, S.: Spray evaporative cooling to achieve ultra fast cooling in runout table. *Int. J. Therm. Sci.* **48**, 1741–1747 (2009)

Corcione, M.: A semi-empirical model for predicting the effective dynamic viscosity of nanoparticle suspensions. *Heat. Transf. Eng.* **33**, 575–583 (2012)

Corcione, M.: Empirical correlating equations for predicting the effective thermal conductivity and dynamic viscosity of nanofluids. *Energy Convers. Manag.* **52**, 789–793 (2011)

Darbha, K.G., Fischer, C., Michler, A., Luetzenkirchen, J., Schäfer, T., Heberling, F., Schild, D.: Deposition of latex colloids at rough

- mineral surfaces: an analogue study using nanopatterned surfaces. *Langmuir* **28**, 6606–6617 (2012)
- Das, S.K., Choi, S.U.S., Yu, W., Pradeep, T.: *Nanofluids science and technology*. John Wiley & Sons, Hoboken, New Jersey (2008)
- Deegan, R.D., Bakajin, O., Dupont, T.F.: Capillary flow as the cause of ring stains from dried liquids. *Nature* **389**, 827–829 (1997)
- Dou, S., Hao, L.: Numerical study of droplet evaporation on heated flat and micro-pillared hydrophobic surfaces by using the lattice Boltzmann method. *Chem. Eng. Sci.* **229**, 116032 (2021)
- Gao, M., Zhang, Da., Kong, P., Zhang, L.-X.: Experimental investigation of Marangoni convection in a sessile droplet at a constant heat flux condition. *Int. Commun. Heat Mass Transfer* **115**, 104600 (2020)
- Gong, W., Yan, Y.Y., Chen, S., Giddings, D.: Numerical study of wetting transitions on biomimetic surface using a lattice Boltzmann approach with large density ratio. *J. Bionic Eng.* **14**, 486–496 (2017)
- Hu, H., Larson, R.G.: Analysis of the microfluid flow in an evaporating sessile droplet. *Langmuir* **21**, 3963–3971 (2005)
- Incropera, F.P., DeWitt, D.P., Bergman, T.L., Lavine A.S.: *Fundamentals of heat and mass transfer*, 6th ed., John Wiley & Sons (2006)
- Jiang, Y.N., Zhou, X.M.: Heat transfer and entropy generation analysis of nanofluids thermocapillary convection around a bubble in a cavity. *Int. Commun. Heat Mass Transfer* **105**, 37–45 (2019a)
- Jiang, Y.N., Zhou, X.M.: Yang Wang, Effects of nanoparticle shapes on heat and mass transfer of nanofluid thermocapillary convection around a gas bubble. *Microgravity Sci. Technol.* **32**, 167–177 (2020)
- Jiang, Y.N., Xu, Z.L.: Numerical Investigation of Nanofluid Thermocapillary Convection Based on Two-Phase Mixture Model. *Microgravity Sci. Technol.* **29**(5), 365–370 (2017)
- Jiang, Y.N., Zhou, X.M.: Numerical study of heat transfer and entropy generation of nanofluids buoyant-thermocapillary convection around a gas bubble. *Microgravity Sci. Technol.* **31**(2), 195–206 (2019b)
- Khanafer, K., Vafai, K.: A critical synthesis of thermophysical characteristics of nanofluids. *Int. J. Heat Mass Transf.* **54**, 4410–4428 (2011)
- Lohani, D., Sarkar, S.: Nanoscale topographical fluctuations: A key factor for evaporative colloidal self-assembly. *Langmuir* **34**, 12751–12758 (2018)
- Manninen, M., Taivassalo, V., Kallio, S.: On the mixture model for multiphase flow, 288, Technical Research Center of Finland. VTT Publications **3**(2), 9–18 (1996)
- Paria, S., Chaudhuri, R.G., Jason, N.N.: Self-assembly of colloidal sulfur particles on a glass surface from evaporating sessile drops: influence of different salts. *New J. Chem.* **38**, 5943–5951 (2014)
- Pham, T., Kumar, S.: Drying of droplets of colloidal suspensions on rough substrates. *Langmuir* **33**, 10061–10076 (2017)
- Pham, T., Kumar, S.: Imbibition and evaporation of droplets of colloidal suspensions on permeable substrates. *Physical Review Fluids* **4**, 034004 (2019)
- Ren, M., Sweelssen, J., Grossiord, N., Gorter, H., Eggenhuisen, T.M., Andriessen, R.: Inkjet printing technology for OPV applications. *J. Imaging Sci. Technol.* **56**(40504–40505), 40504–40501 (2012)
- Saada, M.A., Chikh, S., Tadrist, L.: Evaporation of a sessile drop with pinned or receding contact line on a substrate with different thermophysical properties. *Int. J. Heat Mass Tran* **58**, (2013)
- Schiller, L., Naumann, A.: A drag coefficient correlation. *Z. Ver. Deutsch Ing* **77**(1), 318–320 (1935)
- Sefiane, K., Fukatani, Y., Takata, Y., Kim, J.: Thermal patterns and hydrothermal waves (HTWs) in volatile drops. *Langmuir* **29**, 9750–9760 (2013)
- Sefiane, K., Moffat, J., Matar, O., Craster, R.: Self-excited hydrothermal waves in evaporating sessile drops. *Appl. Phys. Lett.* **93**, 074103 (2008)
- Wang, X., Liu, Z., Wang, Li., Yan, Y.: Investigation of droplet evaporation on copper substrate with different roughness. *J. Bionic Eng.* **17**, 835–842 (2020)
- Xu, X., Luo, J.: Marangoni flow in an evaporating water droplet. *Appl. Phys. Lett.* **91**, 124102–1–3 (2007)
- Ye, S., Wu, C.M., Zhang, L., Li, Y.R., Liu, Q.S.: Evolution of thermal patterns during steady state evaporation of sessile droplets. *Exp. Therm. Fluid Sci.* **98**, 712–718 (2018)
- Ye, S., Zhang, Li., Chun-Mei, Wu., Li, Y.-R., Liu, Q.-S.: Experimental investigation of evaporation dynamic of sessile droplets in pure vapor environment with low pressures. *Int. J. Therm. Sci.* **149**, 106213 (2020)
- Yu, J.-J., Hu, Y.-P., Wu, C.-M., Li, Y.-R., I.B.: Palymskiy, Direct numerical simulations of Rayleigh-Bénard convection of a gas-liquid medium near its density maximum. *App. Thermal. Eng.* **175**, 115387 (2020)
- Yu, J.-J., Li, Z., Li, Y.-R., Chen, J.-C.: Numerical simulations of thermocapillary flow of a binary mixture with the Soret effect in a shallow annular pool. *Microgravity Sci. Technol.* **28**, 1–10 (2016)
- Yu, J.-J., Tang, C.-Y., Li, Y.-R., Qin, T.: Numerical simulation study on the pure solutocapillary flow of a binary mixture with various solutal coefficients of surface tension in an annular pool. *Int. Commun. Heat Mass Transfer* **108**, 104342 (2019)
- Zhang, Y.J., Qian, Y.M., Liu, Z.T., Li, Z.H., Zang, D.Y.: Surface wrinkling and cracking dynamics in the drying of colloidal droplets. *The European Physical Journal E* **37**, 84 (2014)
- Zhou, X.M., Jiang, Y.N., Hou, Y., Du, M.: Thermocapillary Convection Instability in an Annular Two-Layer System under Various Gravity Levels. *Microgravity Sci. Technol.* **31**(5), 641–648 (2019)
- Zu, Y.Q., Yan, Y.Y., Li, J.Q., Han, Z.W.: Wetting behaviors of a single droplet on biomimetic micro structured surfaces. *J. Bionic Eng.* **7**, 191–198 (2010)

Publisher's Note Springer Nature remains neutral with regard to jurisdictional claims in published maps and institutional affiliations.